Chemical Engineering Science 94 (2013) 44–53

Contents lists available at SciVerse ScienceDirect

Chemical Engineering Science

journal homepage: www.elsevier.com/locate/ces

Porosity control in thin film solar cells

Jianqiao Huang [a], Gerassimos Orkoulas [a,*], Panagiotis D. Christofides [a,b]

[a] Department of Chemical and Biomolecular Engineering, University of California, Los Angeles, CA 90095, USA
[b] Department of Electrical Engineering, University of California, Los Angeles, CA 90095, USA

HIGHLIGHTS

- Kinetic Monte Carlo simulation of porous silicon growth process.
- Differential equation model for evolution of porous silicon film site occupancy ratio (SOR).
- Model Predictive Control of film SOR.
- Two stage dual porosity model predictive control system to regulate film SORs of two layers simultaneously.

ARTICLE INFO

Article history:
Received 7 November 2012
Received in revised form
12 February 2013
Accepted 15 February 2013
Available online 28 February 2013

Keywords:
Porous silicon
Dual porosity
Thin film solar cell
Thin film deposition process
Model predictive control

ABSTRACT

This work focuses on the simulation and control of a porous silicon deposition process used in the manufacture of thin film solar cell systems. Initially, a thin film deposition process is simulated via a kinetic Monte Carlo (kMC) method on a triangular lattice following the model developed in Hu et al. (2009). Then a closed-form differential equation model is introduced to predict the dynamics of the kMC model and the parameters in this model are identified by fitting to open-loop kMC simulation results. A model predictive controller (MPC) is also designed and implemented on the kMC model. Extensive closed-loop simulation results demonstrate that both film thickness and porosity can be regulated to desired values. Finally, the porosity control framework is extended into a two-stage dual porosity deposition process, with two different porosity set-points for each stage. The closed-loop results demonstrate that at the end of both stages the film porosity values can be successfully regulated at the requested set-point values.

1. Introduction

It has been widely accepted that solar energy is currently one of the most promising alternative energy sources and thin film silicon solar cells are currently the most widely used solar cell systems. Presently, high costs and limited conversion efficiencies are the main obstacles of a world-wide increase of electric power provided by photovoltaic solar cells (Yerokhov and Melnyk, 1999). Optimizing the light trapping process can be essential in improving the solar cell conversion efficiency and is one of the major research aspects nowadays (e.g. Krč et al., 2003; Müller et al., 2004). It has been found in previous research studies that surface morphology, which includes surface roughness and slope, at each film interface strongly affects the light trapping process (Zeman and Vanswaaij, 2000; Poruba et al., 2000; Huang et al., 2012a,b; Huang et al., 2012c). However, there are some additional problems to be considered in thin film silicon solar cell deposition processes to improve conversion efficiency. On one hand, the materials can be contaminated by various impurities, which might diffuse into the active Si layer during the chemical vapor deposition (CVD) process and result in a degradation of the solar cell light conversion characteristics. On the other hand, the existing substrates may not act as a backside reflector, which is crucial for ultra-thin-film solar cells (Bilyalov et al., 2001, 1999).

One possible way to overcome these problems is to use porous silicon (PS) film as an intermediate layer between the substrate and the thin silicon film (Bilyalov et al., 2001; Vitanov et al., 1997; Yue et al., 2012; Dzhafarov et al., 2012). It has been shown that a single porous silicon layer could serve as a seeding layer and is necessary for a sufficient light reflection (Bilyalov et al., 2001; Krotkus et al., 1997; Najar et al., 2012). Moreover, at the same time this porous silicon layer could be a guttering barrier preventing impurity diffusion from the low-cost substrate into the active silicon layer (Bilyalov et al., 1999). Thus, it is very important to develop a systematic way to simulate and control this porous silicon layer deposition process and improve the solar cell conversion efficiency. Despite its importance, this problem has not attracted much attention.

* Corresponding author. Tel.: +1 310 267 0169; fax: +1 310 206 4107.
E-mail address: makis@seas.ucla.edu (G. Orkoulas).

0009-2509/$ - see front matter © 2013 Elsevier Ltd. All rights reserved.
http://dx.doi.org/10.1016/j.ces.2013.02.046

In the context of modeling and control of thin film microstructure, two mathematical modeling approaches have been developed and widely used: kinetic Monte Carlo (kMC) methods and stochastic differential equation models. KMC methods were initially introduced to simulate thin film microscopic processes. The required thermodynamic and kinetic parameters can be obtained from experiments and molecular dynamics simulations (Levine et al., 1998; Zhang et al., 2004; Levine and Clancy, 2000; Christofides et al., 2008). Since kMC models are not available in closed form, they cannot be readily used for feedback control design and system-level analysis. On the other hand, differential equation models can be derived from the corresponding master equation of the microscopic process and/or identified from process data (Christofides et al., 2008). The closed form of the differential equation models enables their use as the basis for the design of feedback controllers which can regulate thin film porosity and film thickness. Solid-on-solid square lattice models have been frequently used to simulate thin film deposition processes, but in these models no vacancies are allowed inside the film. To this end, in this work, a triangular lattice model, which allows vacancies and overhangs inside the film, is utilized in the simulation.

This work focuses on the development of a model predictive control (MPC) algorithm to simultaneously regulate multiple film site occupancy ratios (SOR) (i.e., film porosity) and the film thickness in a thin film growth process to optimize thin film light trapping. Initially, a thin film deposition process is modeled using the kMC method on a two-dimensional triangular lattice following the model developed in Hu et al. (2009), where vacancies and overhangs are allowed to develop inside the film. This process involves an adsorption process and a migration process in the microscopic scale. A first order ordinary differential equation (ODE) model is used to describe the dynamics of film SOR and predict the evolution of film SOR. A model predictive control algorithm is then developed on the basis of the dynamic equation model to regulate film SOR and thickness at desired levels. Closed-loop simulation results demonstrate the effectiveness of the proposed model predictive control algorithm in successfully regulating the film SOR and thickness to desired levels that optimize thin film light trapping. Finally, a two-stage dual porosity porous silicon deposition process is introduced with two different SOR values for each stage, and closed-loop simulation results demonstrate that both SOR values can be regulated at desired values.

2. Preliminaries

2.1. Triangular-lattice kinetic Monte Carlo model for thin film deposition process

The deposition process is simulated using an on-lattice kMC model via a two-dimensional triangular lattice (Hu et al., 2009), as shown in Fig. 1. The lattice contains a fixed number of sites in the lateral direction. Two microscopic processes are included in the kMC model: an adsorption process, in which particles are incorporated into the film from the gas phase, and a migration process, in which surface particles move to adjacent vacant sites (Levine et al., 1998; Levine and Clancy, 2000; Wang and Clancy, 2001; Yang et al., 1997). The new particles are always deposited from the gas phase; see Fig. 1. The growth direction is normal to the lateral direction. The number of sites in the lateral direction is defined as the lattice size and is denoted by L. Given that the diameter of the silicon atom is around 0.25 nm, the physical size of the lattice can be calculated by $0.25 \times L$.

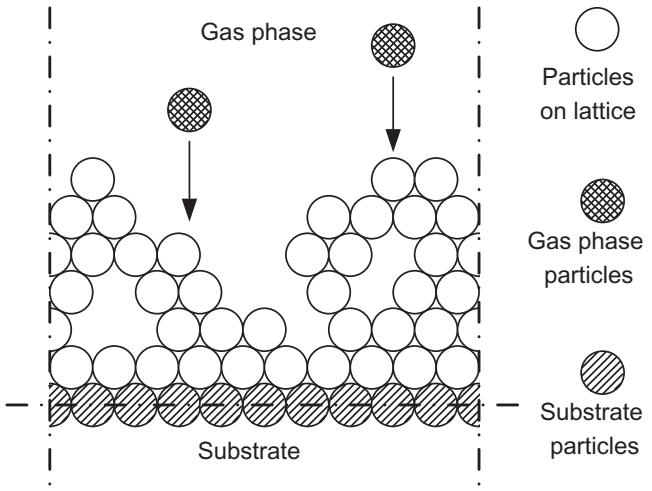

Fig. 1. Thin film growth process on a triangular lattice.

The number of nearest neighbors of a site ranges from zero to six in the triangular lattice model. A site with no nearest neighbors indicates a particle in the gas phase (i.e., a particle which has not been deposited on the film yet). A particle with six nearest neighbors indicates a particle that is fully surrounded by other particles and cannot migrate. A particle with one to five nearest neighbors is possible to diffuse to an unoccupied neighboring site with a probability that depends on its local environment. In the triangular lattice, a particle with only one nearest neighbor is considered unstable and is subject to instantaneous surface relaxation. In the simulation, a bottom layer in the lattice is initially set to be fully packed and fixed, as shown in Fig. 1. There are no vacancies in this layer and the particles in this layer cannot migrate.

2.2. Adsorption process

In an adsorption process, an incident particle is incorporated into the film from the gas phase. The microscopic adsorption rate, W, which is in units of layers per second, depends on the gas phase concentration and is considered as a model input in this work. The length of the lattice, or lattice size L, contains fixed number of particles. In this work, it is assumed that all incident particles have vertical incidence. For the entire deposition process, the microscopic adsorption rate (deposition rate) in terms of incident particles per unit time, which is denoted as r_a, is related to W as follows:

$$r_a = LW \tag{1}$$

The procedure of an adsorption process is illustrated in Fig. 2. After the incident particle, A, is incorporated into the film, it moves to its nearest vacant site, C; if the site is unstable, then this particle relaxes to its nearest stable site, D. Details about the stability and relaxation process of the particles on lattice can be found in Hu et al. (2009). Note that particle surface relaxation is considered as part of the deposition event, and thus, it does not contribute to the process simulation time. There is also only one relaxation event per incident particle.

2.3. Migration process

In a migration process, a particle overcomes the energy barrier of the site and jumps to its vacant neighboring site. The migration rate (probability) of a particle follows an Arrhenius-type law with a pre-calculated activation energy barrier that depends on

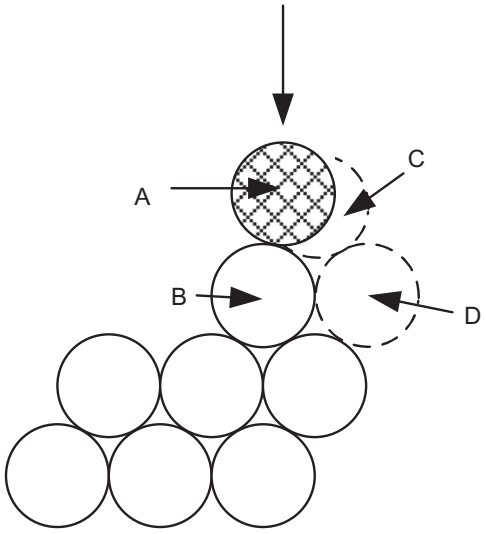

Fig. 2. Schematic of the adsorption event with surface relaxation. In this event, particle A is the incident particle, particle B is the surface particle that is first hit by particle A, site C is the nearest vacant site to particle A among the sites that neighbor particle B, and site D is a stable site where particle A relaxes.

the local environment of the particle, i.e., the number of the nearest neighbors of the particle chosen for a migration event. The migration rate of the ith particle is calculated as follows:

$$r_{m,i} = v_0 \exp\left(-\frac{n_i E_0}{k_B T}\right) \tag{2}$$

where v_0 denotes the pre-exponential factor, n_i is the number of the nearest neighbors of the ith particle and can take the values of 2, 3, 4 and 5 ($r_{m,i}$ is zero when $n_i = 6$ since this particle is fully surrounded by other particles and cannot migrate), E_0 is the contribution to the activation energy barrier from each nearest neighbor, k_B is Boltzmann's constant and T is the substrate temperature of the thin film. Since the film is thin, the temperature is assumed to be uniform throughout the film and is treated as a time-varying but spatially invariant process parameter. In this work, the factor and energy barrier contribution in Eq. (2) take the following values $v_0 = 10^{13}\ s^{-1}$ and $E_0 = 0.9$ eV. These values are appropriate for a silicon film (Keršulis and Mitin, 1995). When a particle is subject to migration, it can jump to one of its vacant neighboring sites with equal probability, unless the vacant neighboring site has no nearest neighbors. Continuous-time Monte Carlo method is used to carry out the simulation and the details of the simulation algorithm can be found in Hu et al. (2009).

2.4. Definition of film site occupancy ratio

Simulations of the kMC model of a porous silicon thin film growth process are implemented utilizing the continuous-time Monte Carlo algorithm. Snapshots of film microstructure, i.e., the configurations of particles within the triangular lattice, are obtained from the kMC model at various time instants during process evolution. To quantitatively evaluate the thin film microstructure, film site occupancy ratio (SOR) is introduced in this subsection. The mathematical expression of film SOR is defined as follows (Hu et al., 2009):

$$\rho = \frac{N}{LH} \tag{3}$$

where ρ denotes the film SOR, N is the total number of deposited particles on the lattice, L is the lattice size, and H denotes the number of deposited layers. Note that the deposited layers are the layers that contain only deposited particles and do not include the initial substrate layers. The variables in the definition expression of Eq. (3) can be found in Fig. 3. Since each layer contains L sites, the total number of sites in the film that can be contained within the H layers is LH. Thus, film SOR is the ratio of the occupied lattice sites, N, over the total number of available sites, LH. Film SOR ranges from 0 to 1. Specifically, $\rho = 1$ denotes a fully occupied film with a flat surface. The value of zero is assigned to ρ at the beginning of the deposition process since there are no particles deposited on the lattice.

Several simulations are carried out to understand the dynamic behavior of SOR at different operating conditions. Fig. 4 shows the SOR dynamic evolution plots at different deposition rates. It is clear that as the deposition rate increases, the film SOR decreases since increased deposition rates leave the particles less time and opportunities for migration. The SOR dynamics dependence on temperature is shown in Fig. 5. As temperature increases, the migration effect becomes stronger and the film particles migrate to increase the film SOR. Fig. 6 shows the system dynamics at different lattice sizes and Fig. 7 shows the SOR steady-state value dependence on lattice size (the SOR steady-state values are

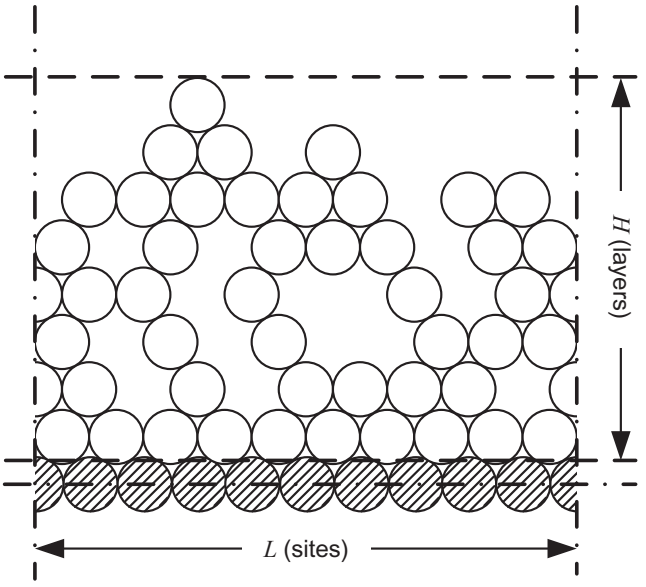

Fig. 3. Illustration of the definition of film SOR of Eq. (3).

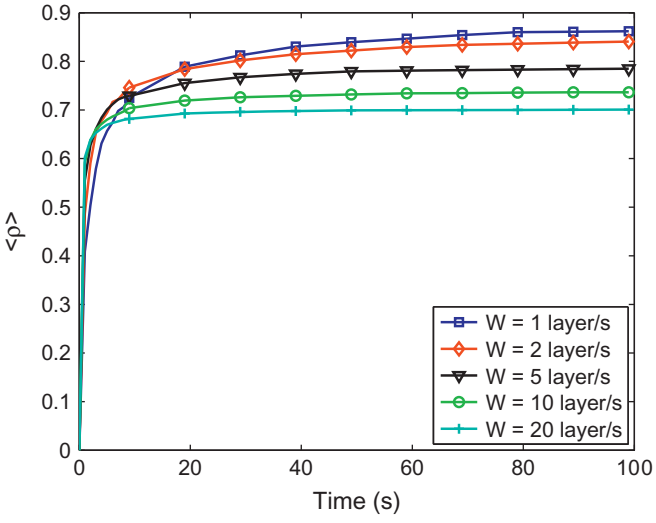

Fig. 4. Time evolution profiles of SOR at different deposition rates.

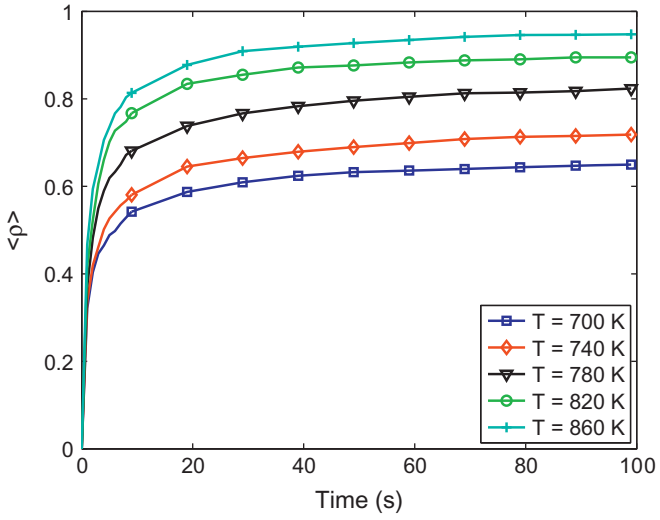

Fig. 5. Time evolution profiles of SOR at different temperatures.

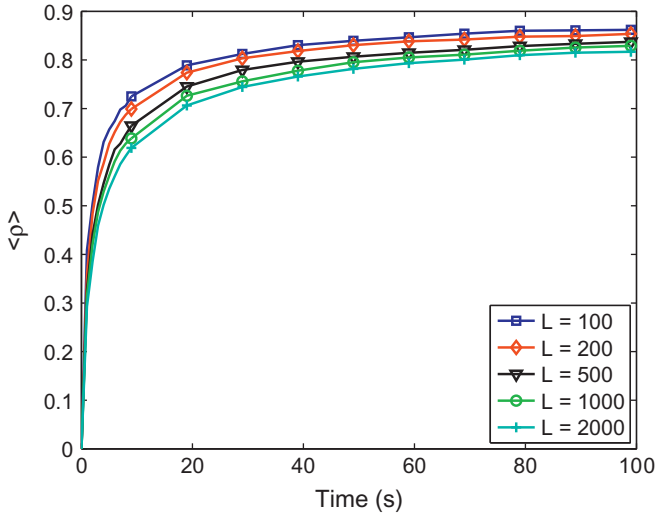

Fig. 6. Time evolution profiles of SOR for different lattice sizes.

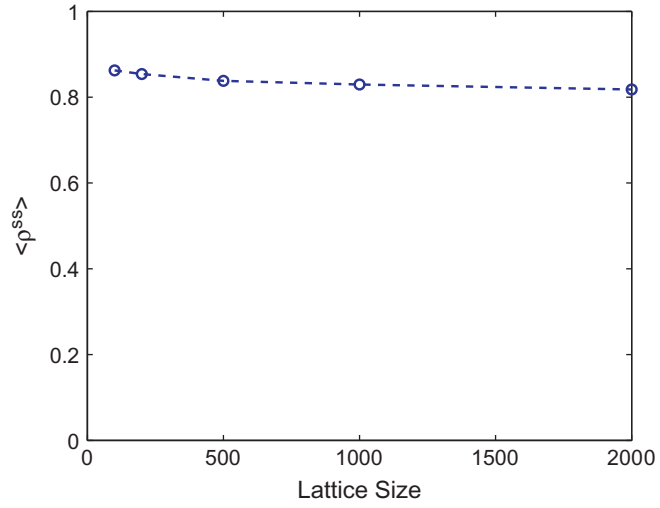

Fig. 7. SOR steady-state value dependence on lattice size.

approximated by averaging the last 10 values of SOR evolution profiles). It is clear in this plot that lattice size has very limited influence over system SOR dynamics, so in this work using a small lattice size ($L=100$) to carry out the simulations will not affect the results and the conclusions.

3. Dynamic model construction and parameter estimation

3.1. Dynamic model of film site occupancy ratio

As already emphasized, film porosity is characterized by the site occupancy ratio (SOR). According to the definition of film SOR of Eq. (3), film SOR accounts for all deposited layers during the entire deposition process. Since film SOR is a cumulative property, its evolution can be characterized by an integral form. Before further derivation of the dynamic model of film SOR, the concept of instantaneous film SOR of the film layers deposited between time t and $t+\Delta t$, denoted by ρ_d, is first introduced as the spatial derivative of the number of deposited particles in the growing direction as follows:

$$\rho_d = \frac{dN}{d(HL)} \tag{4}$$

In Eq. (4), the lattice size L is a constant and the derivative dH can be written as a linear function of time derivative dt as follows:

$$dH = r_H\, dt \tag{5}$$

where r_H is the growth rate of the thin film from the top layer point of view. The expressions of N and H can be obtained by integrating equations (4) and (5) as follows:

$$N(t) = L\int_0^t \rho_d r_H\, ds$$

$$H(t) = \int_0^t r_H\, ds \tag{6}$$

With the definition of ρ of Eq. (3) and the expressions of N and H of Eq. (6), the film SOR of Eq. (3) can be rewritten in an integral form as follows:

$$\rho = \frac{\int_0^t \rho_d r_H\, ds}{\int_0^t r_H\, ds} \tag{7}$$

To simplify the subsequent development and develop an SOR model that is suitable for control purposes, we assume that the dynamics of the instantaneous film SOR, ρ_d, can be approximated by a first-order process, i.e.:

$$\tau\frac{d\rho_d(t)}{dt} = \rho_d^{ss} - \rho_d(t) \tag{8}$$

where τ is the time constant and ρ_d^{ss} is the steady-state value of the instantaneous film SOR. We note that the first-order ODE model of Eq. (8) was introduced and justified with numerical results in Hu et al. (2009) for the modeling of the partial film SOR, which is defined to characterize the evolution of the film porosity of layers that are close to the film surface. In this sense, the instantaneous film SOR is a similar concept to the partial film SOR, because it also describes the contribution to the bulk film porosity of the newly deposited layers. Therefore, the first-order ODE model is a suitable choice to describe the evolution of the instantaneous film SOR.

From Eq. (7), it follows that at large times as ρ_d approaches ρ_d^{ss}, the steady-state film SOR (ρ^{ss}) approaches the steady-state value of the instantaneous film SOR (i.e., $\rho^{ss}=\rho_d^{ss}$). The deterministic ODE system of Eq. (8) is subject to the following initial condition:

$$\rho_d(t_0) = \rho_{d0} \tag{9}$$

where t_0 is the initial time and ρ_{d0} is the initial value of the instantaneous film SOR. From Eqs. (8) and (9) and the fact that

$\rho^{ss} = \rho_d^{ss}$ at large times, it follows that

$$\rho_d(t) = \rho^{ss} + (\rho_{d0} - \rho^{ss}) e^{-(t-t_0)/\tau}. \tag{10}$$

For controller implementation purposes, the expression of the film SOR can be derived as follows:

$$\rho(t) = \frac{\int_0^{t_0} \rho_d r_H \, ds + \int_{t_0}^{t} \rho_d r_H \, ds}{\int_0^{t_0} r_H \, ds + \int_{t_0}^{t} r_H \, ds} = \frac{\rho(t_0) H(t_0) + \int_{t_0}^{t} \rho_d r_H \, ds}{H(t_0) + \int_{t_0}^{t} r_H \, ds} \tag{11}$$

where t_0 is the current time, $\rho(t_0)$ and $H(t_0)$ are the film SOR and the film height at time t_0, respectively.

Substituting the solution of ρ_d of Eq. (10) into Eq. (11) and assuming that r_H is constant for $t > \tau > t_0$, which is taken to be the case in the parameter estimation and the MPC formulations below, the analytical solution of film SOR at time t can be obtained as follows:

$$\rho = \frac{\rho(t_0) H(t_0) + r_H[\rho^{ss}(t-t_0) + (\rho^{ss} - \rho(t_0))\tau(e^{-(t-t_0)/\tau} - 1)]}{H(t_0) + r_H(t-t_0)} \tag{12}$$

which is directly utilized in the model predictive control formulation of Eq. (13).

3.2. Parameter estimation

In the dynamic model of Eq. (8), there are two model parameters that need to be obtained from kMC data of the deposition process. These model parameters can be estimated on the basis of the open-loop simulation data at fixed deposition rates from the kMC model introduced in Section 2 by using least-square methods (Hu et al., 2009). In the parameter estimation, the predicted evolution profiles from the dynamic model of Eq. (8) and the ones from the kMC simulation of the deposition process are compared in a least-square sense to find the best model parameters.

Different operating conditions strongly affect the deposition process and result in different dynamics of the surface height profile and of the film SOR. Thus, the model parameters are functions of the operating conditions. In this work, we choose the deposition rate, W, as the manipulated input and keep the substrate temperature fixed at $T=800$ K. Fig. 8 shows the closed form ODE model dynamics fitted to open-loop kMC simulations. It is clear that the closed-form model can accurately predict the SOR profile obtained from the kMC simulation. The dependence of the

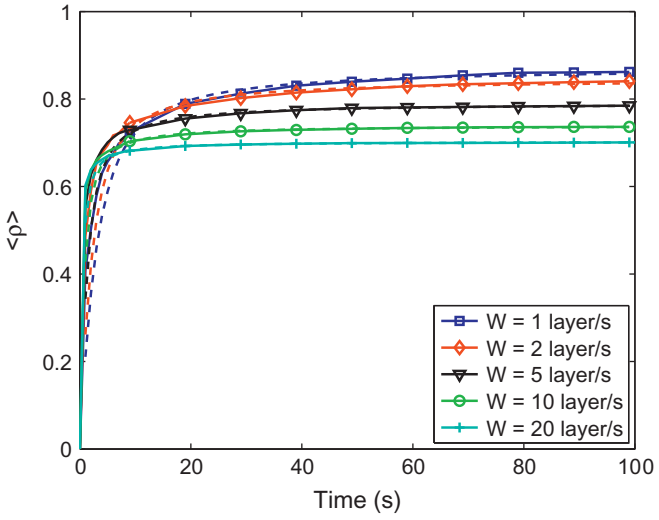

Fig. 8. Closed-form model fitted to open-loop kMC simulation results.

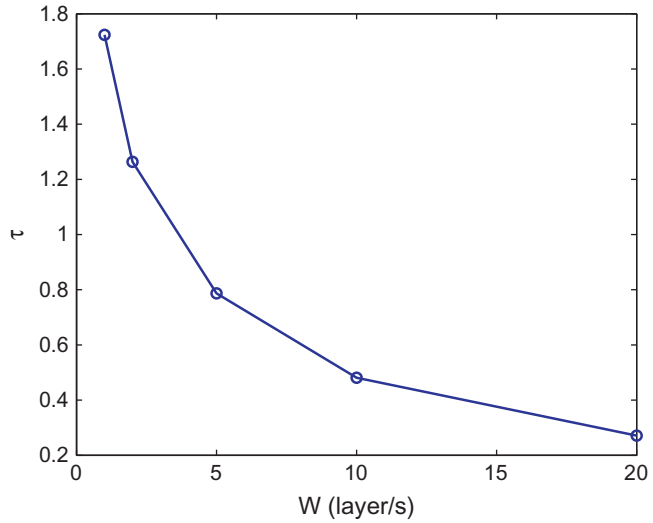

Fig. 9. Dependence of τ on the deposition rate with substrate temperature $T=800$ K.

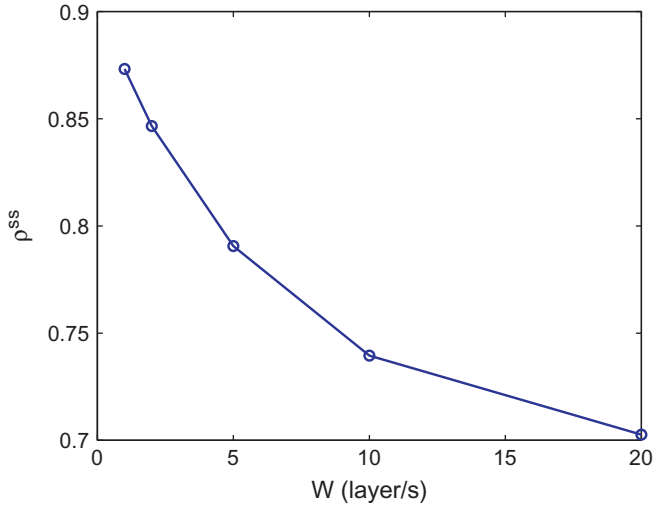

Fig. 10. Dependence of ρ_{ss} on the deposition rate with substrate temperature $T=800$ K.

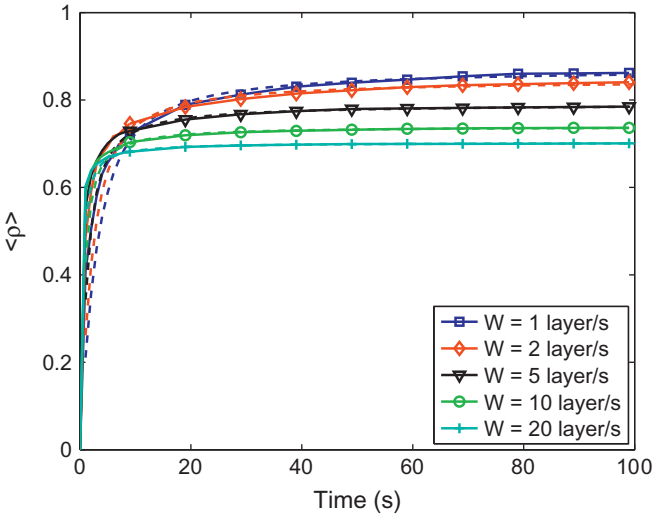

Fig. 11. Evolution of expected film SOR at different deposition rates from the kMC model (solid lines with symbols) and expected aggregate roughness solutions from the corresponding closed-form equations (dashed lines).

model parameters on the deposition rate, W, can be obtained by performing the parameter estimation procedure discussed above for a variety of deposition rate values (ranging from 1 to 20 layer/s); see Figs. 9 and 10 for the dependence of the model parameters on the deposition rate. Simulation results from 100 independent simulation runs are used for the parameter estimation under each deposition rate condition. It can be clearly seen that the model parameters are strong functions of the deposition rate and this dependence is the basis for using W to simultaneously control film thickness and porosity. After parameter estimation, it is necessary to verify whether or not the obtained closed-form model can be used to predict the kMC simulation results. Thus, film SOR evolution profiles, which are obtained from the closed-form model of Eq. (8) at different operating conditions, are compared with open-loop kMC simulation results, as is shown in Fig. 11. It is clear that the closed-form model profiles fit the open-loop kMC simulation results very well, and this demonstrates that the proposed closed-form model can be used to predict the process dynamics for control purposes.

4. Model predictive controller design

In this section, a model predictive controller (MPC) is designed based on the dynamic model of film SOR to regulate the expected values of film thickness and SOR to desired levels by manipulating the deposition rate. The value of film SOR and thickness is assumed to be available to the controller. In practice, real-time estimates of film porosity can be obtained from a combination of in situ gas phase measurements and off-line thin film porosity measurements. While it is difficult to obtain real-time direct measurements of film porosity, it is possible to use open-loop experimental data at different deposition conditions (including off-line porosity measurements) to construct a model that estimates film porosity from in-situ gas phase measurements and combine this model with the model predictive control system proposed in this work; the reader may refer to Ni et al. (2004) for an experimental implementation of this approach in the context of thin film carbon content measurement and control.

4.1. MPC formulation

We consider the control problem of film thickness and film porosity by using a model predictive control design. The expected values, $\langle \overline{h} \rangle$ and $\langle \rho \rangle$, are chosen as the control objectives. The deposition rate is used as the manipulated input. In practice, the deposition rate can be manipulated by changing the inlet flow rates to the deposition process. The substrate temperature is fixed at a certain value, $T_0 = 800$ K, during all closed-loop simulations. It is necessary to point out that both the deposition rates and the temperature strongly influence the evolution of thin films and either or both can be used as manipulated variables. In the present case, we fix $T = 800$ K because there are available experimental data in this temperature for porosity that allowed us to fine-tune our kMC model and subsequently, the deposition rate became the natural choice for manipulated input which also allows us to reach a broad range of porosity values. We note here that the proposed modeling and control methods do not depend on the specific number of the manipulated variables and can be easily extended to the case of multiple inputs. To account for a number of practical considerations, several constraints are added to the control problem. First, there is a constraint on the range of variation of the deposition rate. Another constraint is imposed on the rate of change of the deposition rate to account for actuator limitations. The control action at time t is obtained by solving an optimal control problem.

The cost function in the optimal control problem includes penalty on the deviation of $\langle \overline{h} \rangle$ and $\langle \rho \rangle$ from their respective set-point values. Different weighting factors are assigned to the penalties on the deviations of the film height and of the film SOR. Relative deviations are used in the formulation of the cost function to make the magnitude of the different terms used in the cost comparable for numerical calculation purposes. The optimal profile of the deposition rate is calculated by solving an optimization problem in a receding horizon fashion. Specifically, the MPC problem is formulated as follows:

$$
\begin{aligned}
&\min_{W_1,\ldots,W_i,\ldots,W_p} J = \sum_{i=1}^{p} (q_{h,i} F_{h,i} + q_{\rho,i} F_{\rho,i}) \\
&\text{s.t.} \\
&F_{h,i} = \left[\frac{h_{set} - \langle h(t_i) \rangle}{h_{set}} \right]^2 \\
&F_{\rho,i} = \left[\frac{\rho_{set} - \rho(t_i)}{\rho_{set}} \right]^2 \\
&\langle \overline{h}(t_i) \rangle = \langle \overline{h}(t_{i-1}) \rangle + r_h \Delta \\
&\rho(t_i) = \frac{\rho(t_{i-1}) \langle \overline{h}(t_{i-1}) \rangle + r_h [\rho^{ss} \Delta + (\rho^{ss} - \rho(t_{i-1})) \tau (e^{-\Delta/\tau} - 1)]}{\langle \overline{h}(t_{i-1}) \rangle + r_h \Delta} \\
&W_{min} < W_i < W_{max}, \quad \left| \frac{W_{i+1} - W_i}{\Delta} \right| \le L_W, \quad i = 1,2,\ldots,p
\end{aligned}
\tag{13}
$$

where t is the current time, Δ is the sampling time, p is the number of prediction steps, $p\Delta$ is the specified prediction horizon, t_i, $i=1, 2,\ldots,p$, is the time of the ith prediction step ($t_i = t + i\Delta$), respectively, W_i, $i=1, 2,\ldots,p$, is the deposition rate at the ith step ($W_i = W(t + i\Delta)$), respectively, $q_{h,i}$, and $q_{\rho,i}$, $i=1, 2,\ldots,p$, are the weighting penalty factors for the deviations of $\overline{h}$ and ρ from their respective set-points $\overline{h}_{set}$ and ρ_{set} at the ith prediction step, W_{min} and W_{max} are the lower and upper bounds on the deposition rate, respectively, and L_W is the limit on the rate of change of the deposition rate.

The dependence of the model parameters, r_h, ρ^{ss}, and τ, on the deposition rate, W, of Eq. (13) is used in the formulation of the model predictive controller. The parameters estimated under time-invariant operating conditions are suitable for the purpose of MPC design because the control input in the MPC formulation is piecewise constant, i.e., the manipulated deposition rate remains constant between two consecutive sampling times, and thus, the dynamics of the microscopic process can be predicted using the dynamic models with the estimated parameters for the fixed value of W.

5. Simulation results

In this section, the proposed model predictive controller of Eq. (13) is applied to the kMC model of the thin film growth process described in Section 2. The value of the deposition rate is obtained from the solution of the problem of Eq. (13) at each sampling time and is applied to the closed-loop system until the next sampling time. The optimization problem in the MPC formulation of Eq. (13) is solved via a local constrained minimization algorithm using a broad set of initial guesses.

The substrate temperature is fixed at 800 K and the initial deposition rate is 1.0 layer/s. The variation of deposition rate is from 1.0 layer/s to 20.0 layer/s. The maximum rate of change of the deposition rate is $L_W = 1$ layer/s^2. Both penalty factors, $q_{h,i}$, and $q_{\rho,i}$, are set to be either zero or one. The time interval between two measurement samplings is 1 s. The closed-loop simulation duration is 100 s. All expected values are obtained from 100 independent simulation runs.

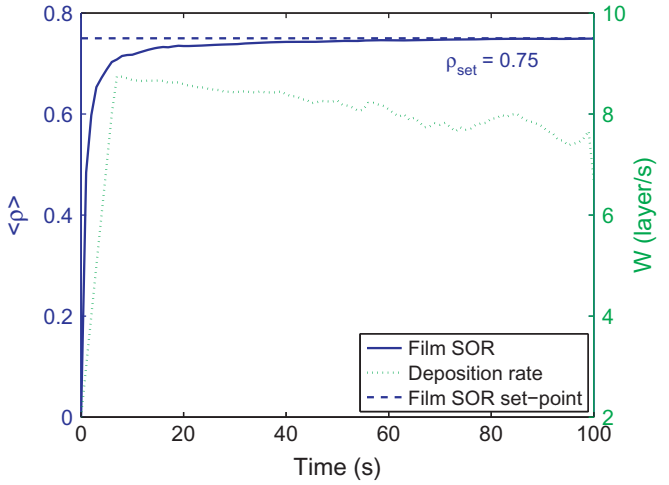

Fig. 12. Profiles of film SOR (solid line) and of the deposition rate (dotted line) under closed-loop operation; SOR-only control with $\rho_{set} = 0.75$.

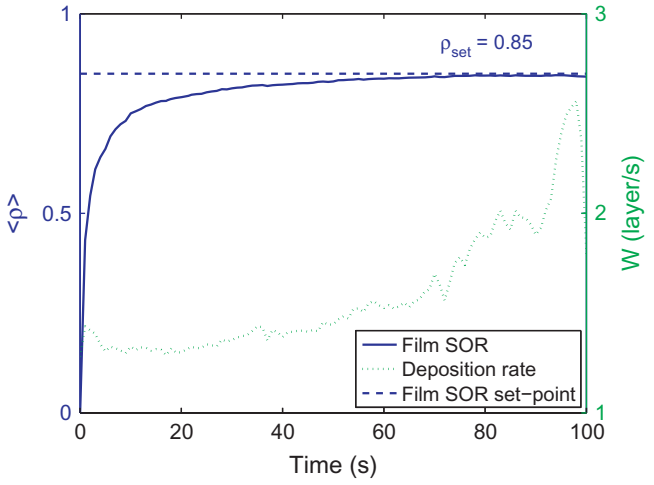

Fig. 14. Profiles of film SOR (solid line) and of the deposition rate (dotted line) under closed-loop operation; SOR-only control with $\rho_{set} = 0.85$.

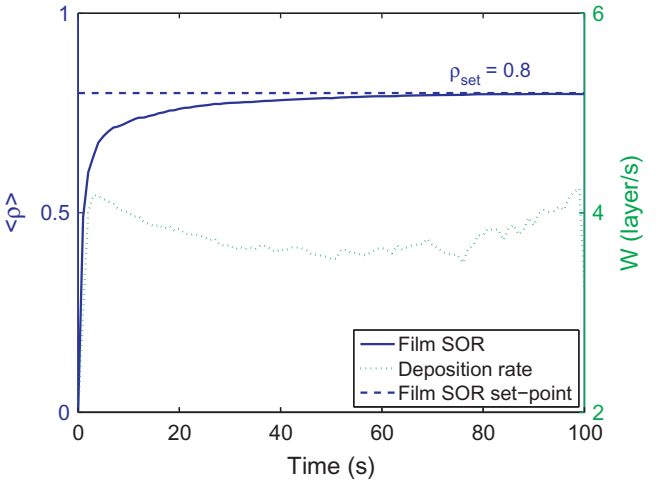

Fig. 13. Profiles of film SOR (solid line) and of the deposition rate (dotted line) under closed-loop operation; SOR-only control with $\rho_{set} = 0.8$.

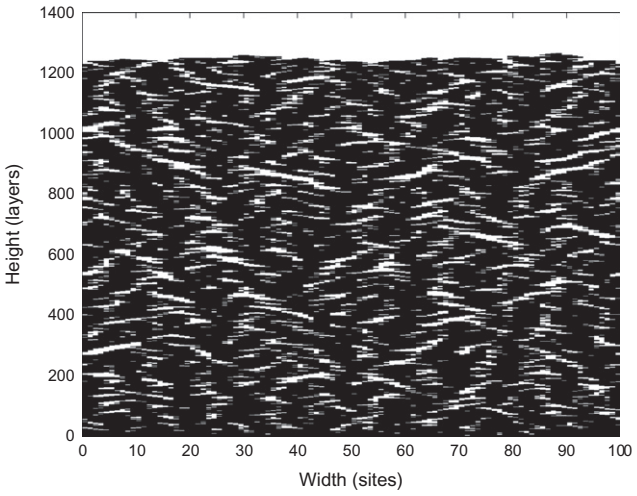

Fig. 15. Film snapshot when $\rho = 0.75$.

5.1. Regulation of film porosity by manipulating deposition rate

In this subsection, film SOR is the control objective (porosity control problem). In the porosity control problem, the cost function in the MPC formulation includes only penalty on the deviation of the expected value of film SOR from the set-point value. Figs. 12–14 show the evolution profiles of the expected film SOR from the closed-loop simulations of the porosity control problem and the corresponding input deposition rate profile from one run. These set-points range from $\rho = 0.75$ to $\rho = 0.85$, which is the commonly desired range for improved light trapping performance (Bilyalov et al., 1999, 2001). The model predictive controller successfully drives the expected film SORs to the set-point values. Specifically, in Fig. 12, by checking Fig. 4, the optimal input for deposition rate should be around 10 layer/s. Since the initial value of deposition rate is 2 layer/s and the maximum change between two steps is 1 layers/s^2, during the first several steps, the change of deposition rate is restricted by the input rate-of-change constraint, so it takes multiple sampling times for the control system to reach its optimal deposition rate. At the end of the simulation, the input is close to zero given that the SOR almost reaches the set-point. Similar dynamic behaviors can also be observed from the other plots.

In order to get a more intuitive understanding of the difference in the SOR, two film snapshots obtained for $\rho = 0.75$ and $\rho = 0.85$ are shown in Figs. 15 and 16, respectively. Since the heights of these two snapshots are very different, it is hard to directly compare the SOR differences. Thus, Fig. 15 is enlarged and only the top 200 layers are shown in Fig. 17. It is clear that the film SOR in Fig. 17 is clearly lower than the film SOR in Fig. 16.

5.2. Simultaneous regulation of film thickness and porosity

Simultaneous regulation of film thickness and film SOR is long desired in porous silicon production (Yerokhov and Melnyk, 1999). Closed-loop simulations of simultaneous regulation of film thickness and film SOR are also carried out. Fig. 18 shows the simulation results for this case, and the input deposition rate profile is shown in Fig. 19. The expected values of both film height and film SOR approach their corresponding set-points with a small trade off. Since the deposition rate is the only manipulated variable, there is no guarantee that both control objectives can be achieved for a given film thickness over a 100-second deposition process duration.

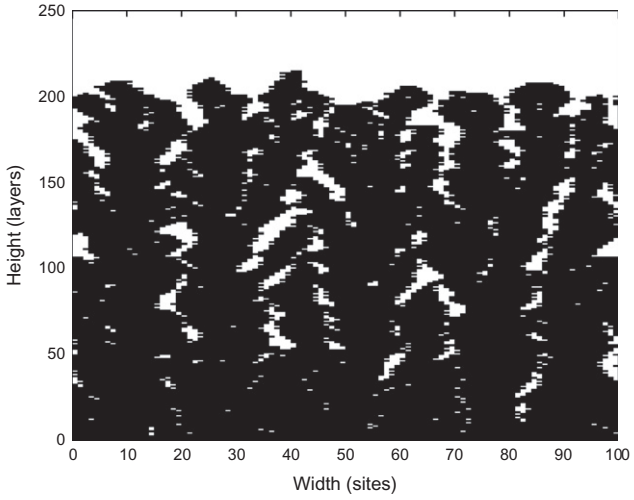

Fig. 16. Film snapshot when $\rho = 0.85$.

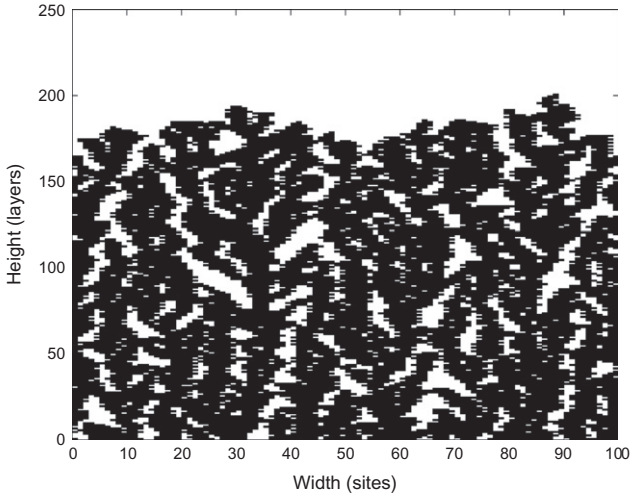

Fig. 17. Film snapshot when $\rho = 0.75$ (top 200 layers).

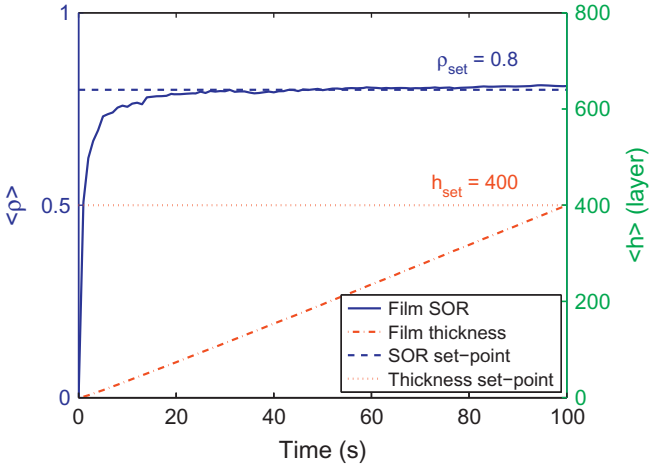

Fig. 18. Profiles of film SOR (solid line) and of the film thickness (dash-dotted line) under closed-loop operation; simultaneous regulation of film thickness and SOR with $\rho_{set} = 0.8$ and $h_{set} = 400$.

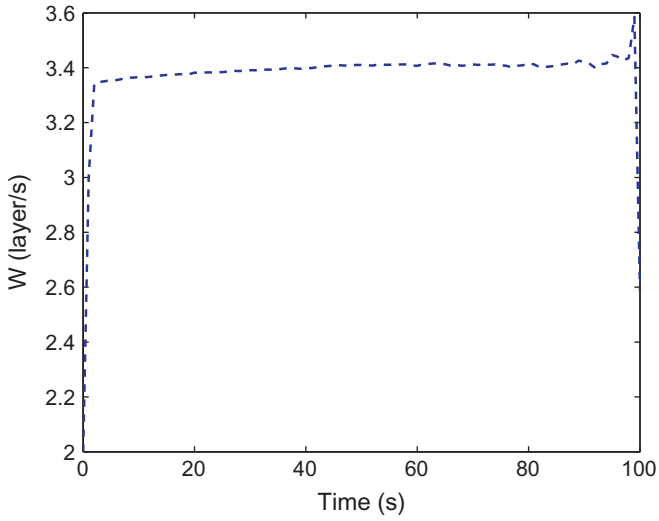

Fig. 19. Profile of input deposition rate under simultaneous regulation of film thickness and SOR with $\rho_{set} = 0.8$ and $h_{set} = 400$.

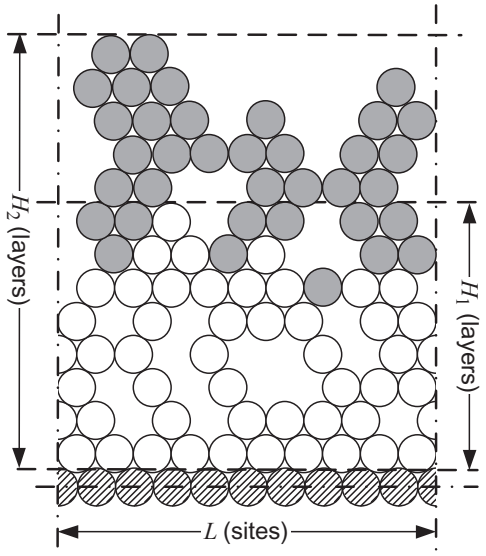

Fig. 20. Illustration of the definition of film SOR of dual porosity film deposition process.

5.3. Dual porosity regulation with model predictive controller

In solar panel industry, it is very common to use dual porosity silicon layers between the substrate and the thin silicon film (Bilyalov et al., 2001; Jin et al., 2000). Dual porosity silicon layers are composed of two independent layers with different SOR values. Our existing modeling and control framework is extended to simulate and control such a dual porosity deposition process. The extended process is divided into two stages, as is shown in Fig. 20. Stage One is exactly the same process as discussed in Fig. 3, and at the end of Stage One, the height H_1 is recorded. In Stage Two, the film SOR is defined as

$$\rho = \frac{N'}{L(H_2 - H_1)} \tag{14}$$

where N' is the number of particles deposited above H_1. $L(H_2-H_1)$ is the maximum number of particles that can be deposited in this area. It is necessary to point out that at the beginning of Stage Two, some particles can deposit into the area below H_1, as is shown in Fig. 20; as a result, the defined SOR value can be larger than one. To avoid creating an inconsistency in the SOR value, at the beginning of Stage

Two, no new control (optimization) problem will be solved until the heights of all lattice columns are higher than H_1 and the control action is maintained at the last calculated value. Specifically, during this period of time, the constant control input from the last step of

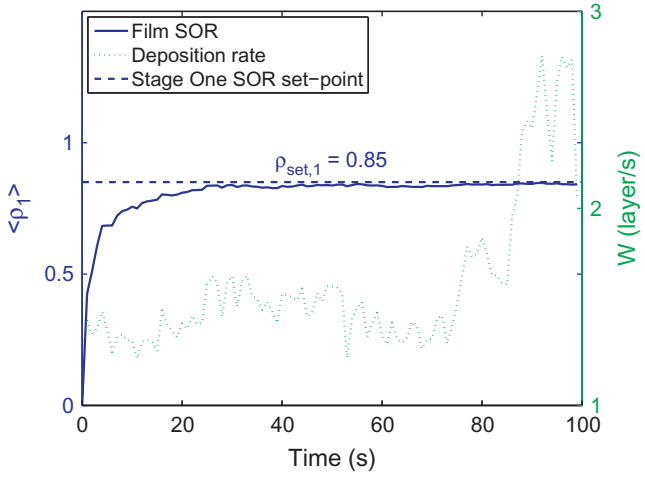

Fig. 21. Profiles of film SOR (solid line) and of the deposition rate (dotted line) under two-stage dual porosity closed-loop operation (stage one).

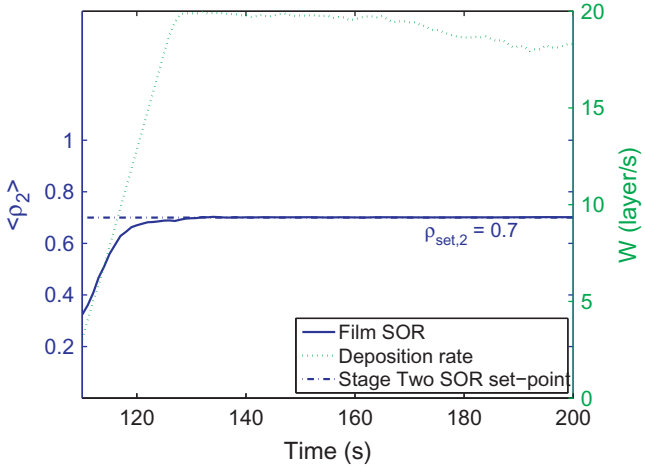

Fig. 22. Profiles of film SOR (solid line) and of the deposition rate (dotted line) under two-stage dual porosity closed-loop operation (stage two).

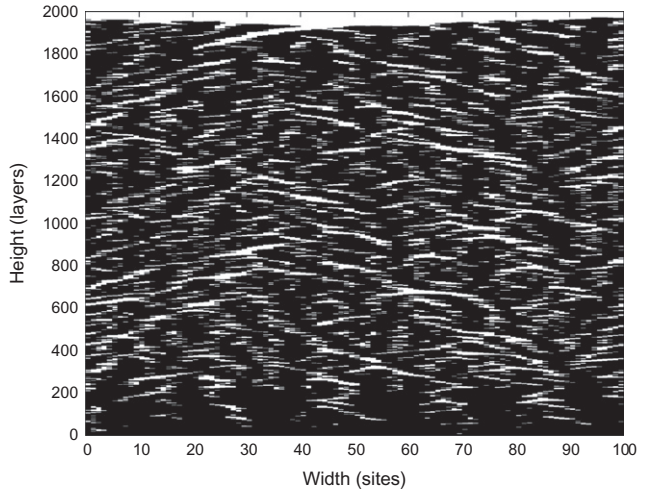

Fig. 23. Film snapshot of two-stage dual porosity closed-loop system.

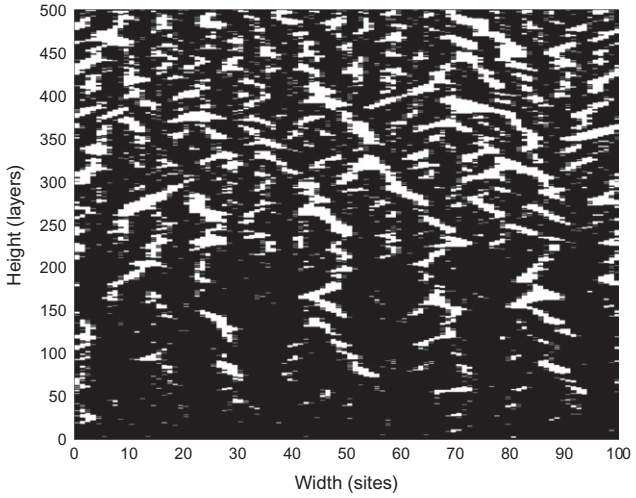

Fig. 24. Interface snapshot of two-stage dual porosity closed-loop system.

Stage One is applied to the kMC simulation and the SOR definition from Stage One is utilized to calculate the film SOR.

Closed-loop simulations are carried out to demonstrate this two-stage dual porosity control framework. The simulation time for both periods is $t_1 = t_2 = 100$ s; set points for both stages are picked as $\rho_{set,1} = 0.85$ and $\rho_{set,2} = 0.7$. As is shown in Figs. 21 and 22, film SOR reaches its set-point at the end of Stage One; during the following several seconds (10 s in this simulation), since the heights of some columns are still lower than H_1 in Fig. 20, no new control (optimization) problem is solved and the control input from the last step of Stage One is applied to the system. After the heights of all columns are higher than H_1, new control inputs are calculated and film SOR is driven to $\rho_{set,2}$ successfully at the end of Stage Two. The film snapshot of this simulation is obtained and shown in Fig. 23. The deposition rate in Stage One is around 2 layer/s and the deposition rate in Stage Two is around 18 layer/s so the depth of these two layers is very different. To have a more intuitive view of the film SOR, the film interface snapshot is obtained and shown in Fig. 24. It is clear that the film SOR of the upper layer is lower than that of the bottom layer.

6. Conclusions

In this work, a porous silicon thin film deposition process used in the manufacture of thin film solar cells is considered. The process is initially simulated via the kinetic Monte Carlo (kMC) method on a triangular lattice. Then a closed form differential equation model is introduced to predict the dynamics of film porosity and the parameters in this model are identified by fitting to open-loop kMC simulation results. A model predictive controller (MPC) is designed and multiple set-points are picked to demonstrate the controller performance. Results demonstrate that both film thickness and SOR can be regulated to experimentally determined set-points. Finally, a two-stage dual porosity control framework is proposed to generate a dual porosity silicon thin film with desired film SORs in the two distinct layers.

Acknowledgement

Financial support from the National Science Foundation, CBET-0652131, and a UCLA Doctoral Dissertation Year Fellowship to Jianqiao Huang are gratefully acknowledged.

References

Bilyalov, R., Stalmans, L., Beaucarne, G., Loo, R., Caymax, M., Poortmans, J., Nijs, J., 2001. Porous silicon as an intermediate layer for thin-film solar cell. Sol. Energy Mater. Sol. Cells 65, 477–485.

Bilyalov, R., Stalmans, L., Schirone, L., Levy-Clement, C., 1999. Use of porous silicon antireflection coating in multicrystalline silicon solar cell processing. IEEE Trans. Electron Devices 46, 2035–2040.

Christofides, P.D., Armaou, A., Lou, Y., Varshney, A., 2008. Control and Optimization of Multiscale Process Systems. Birkhäuser, Boston.

Dzhafarov, T.D., Aslanov, S.S., Ragimov, S.H., Sadigov, M.S., Yuksel, S.A., 2012. Effect of nanoporous silicon coating on silicon solar cell performance. Vacuum 86, 1875–1879.

Hu, G., Orkoulas, G., Christofides, P.D., 2009. Modeling and control of film porosity in thin film deposition. Chem. Eng. Sci. 64, 3668–3682.

Huang, J., Orkoulas, G., Christofides, P.D., 2012a. Modeling and control of transparent conducting oxide layer surface morphology for improved light trapping. Chem. Eng. Sci. 74, 135–147.

Huang, J., Orkoulas, G., Christofides, P.D., 2012b. Simulation and control of aggregate surface morphology in a two-stage thin film deposition process for improved light trapping. Chem. Eng. Sci. 71, 520–530.

Huang, J., Orkoulas, G., Christofides, P.D., 2012c. Surface morphology control of transparent conducting oxide layers for improved light trapping using wafer grating and feedback control. Chem. Eng. Sci. 81, 191–201.

Jin, S., Bender, H., Stalmans, L., Bilyalov, R., Poortmans, J., Loo, R., Caymax, M., 2000. Transmission electron microscopy investigation of the crystallographic quality of silicon films grown epitaxially on porous silicon. J. Crystal Growth 212, 119–127.

Keršulis, S., Mitin, V., 1995. Monte Carlo simulation of growth and recovery of silicon. Mater. Sci. Eng. B 29, 34–37.

Krotkus, A., Grigorasa, K., Paebutasa, V., Barsonyb, I., Vazsonyib, B., Friedb, M., Szlufcikc, J., Nijsc, J., Levy-Clement, C., 1997. Efficiency improvement by porous silicon coating of multicrystalline solar cells. Sol. Energy Mater. Sol. Cells 45, 267–273.

Krč, J., Smole, F., Topič, M., 2003. Analysis of light scattering in amorphous Si: H solar cells by a one-dimensional semi-coherent optical model. Prog. Photovolt.: Res. Appl. 11, 15–26.

Levine, S.W., Clancy, P., 2000. A simple model for the growth of polycrystalline Si using the kinetic Monte Carlo simulation. Model. Simul. Mater. Sci. Eng. 8, 751–762.

Levine, S.W., Engstrom, J.R., Clancy, P., 1998. A kinetic Monte Carlo study of the growth of Si on Si(100) at varying angles of incident deposition. Surf. Sci. 401, 112–123.

Müller, J., Rech, B., Springer, J., Vanecek, M., 2004. TCO and light trapping in silicon thin film solar cells. Sol. Energy 77, 917–930.

Najar, A., Charrier, J., Pirasteh, P., Sougrat, R., 2012. Ultra-low reflection porous silicon nanowires for solar cell applications. Opt. Express 20, 16861–16870.

Ni, D., Lou, Y., Christofides, P.D., Sha, L., Lao, S., Chang, J.P., 2004. Real-time carbon content control for PECVD ZrO_2 thin-film growth. IEEE Trans. Semic. Manuf. 17, 221–230.

Poruba, A., Fejfar, A., Remeš, Z., Špringer, J., Vaněček, M., Kočka, J., 2000. Optical absorption and light scattering in microcrystalline silicon thin films and solar cells. J. Appl. Phys. 88, 148–160.

Vitanov, P., Kamenova, M., Tyutyundzhiev, N., Delibasheva, M., Goranova, B., Peneva, M., 1997. High-efficiency solar cell using a thin porous silicon layer. Thin Solid Films 297, 299–303.

Wang, L., Clancy, P., 2001. Kinetic Monte Carlo simulation of the growth of polycrystalline Cu films. Surf. Sci. 473, 25–38.

Yang, Y.G., Johnson, R.A., Wadley, H.N., 1997. A Monte Carlo simulation of the physical vapor deposition of nickel. Acta Mater. 45, 1455–1468.

Yerokhov, V.Y., Melnyk, I.I., 1999. Porous silicon in solar cell structures: a review of achievements and modern directions of further use. Renew. Sustain. Energy Rev. 3, 291–322.

Yue, Z., Shen, H., Zhang, L., Liu, B., Gao, C., Lv, H., 2012. Heterojunction solar cells produced by porous silicon layer transfer technology. Appl. Phys. A: Mater. Sci. Process. 108, 929–934.

Zeman, M., Vanswaaij, R., 2000. Optical modeling of a-Si:H solar cells with rough interfaces: effect of back contact and interface roughness. J. Appl. Phys. 88, 6436–6443.

Zhang, P., Zheng, X., Wu, S., Liu, J., He, D., 2004. Kinetic Monte Carlo simulation of Cu thin film growth. Vacuum 72, 405–410.